

SUPPORTING INFORMATION

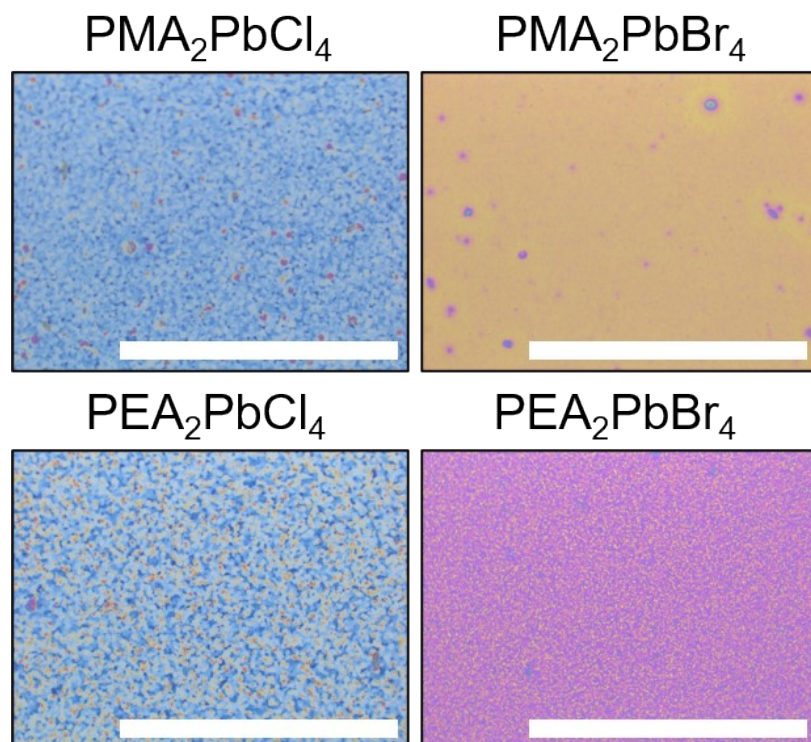
Utilizing 2D metal halide perovskite thin films as highly tunable surfaces for crystallographic orientation control of energetic materials

Natalie Smith-Papin^a, Meagan Phister^a, Ashley Conley^a, Nathan Swami^b, Zbigniew Dreger^b, Gaurav Giri^{a}*

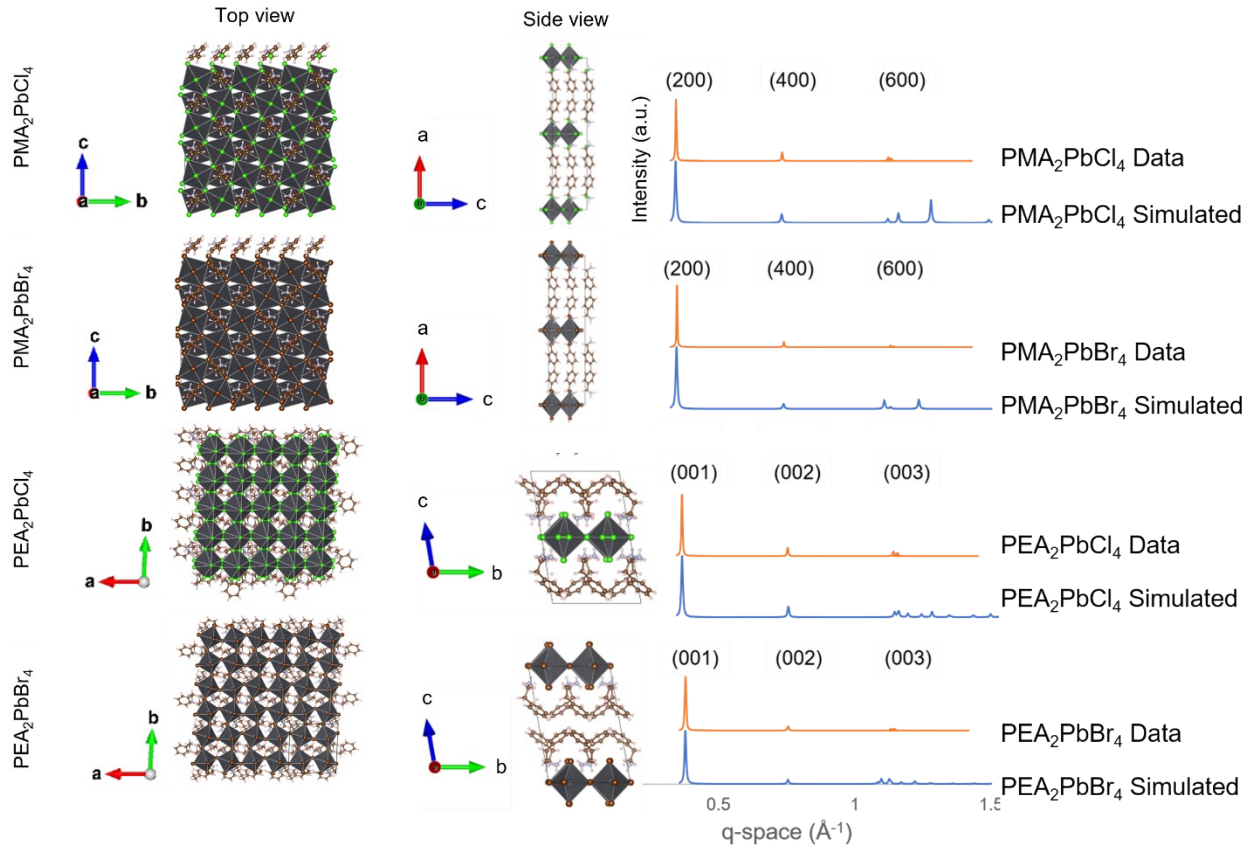
^a Department of Chemical Engineering, University of Virginia, Charlottesville, Virginia, 22904, United States

^b Department of Electrical and Computer Engineering, University of Virginia, Charlottesville, Virginia, 22904, USA.

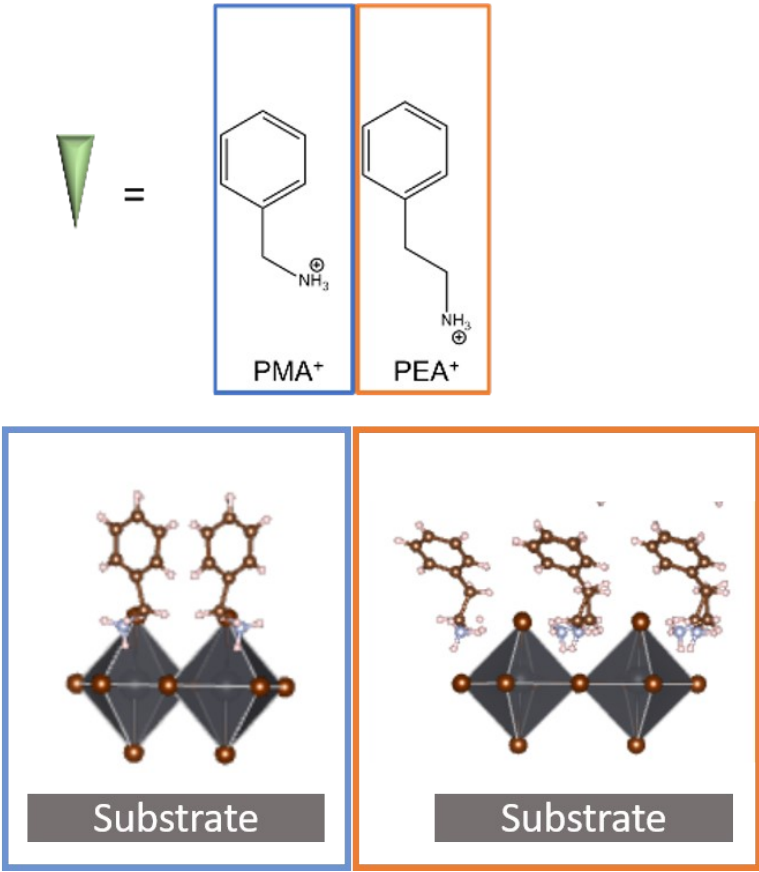
^c RDT&E Department, Naval Surface Warfare Center Indian Head Division, Indian Head, Maryland 20640, United States



SI Figure 1: Optical images of spincoated perovskite films. Scale bar = 200 μm.



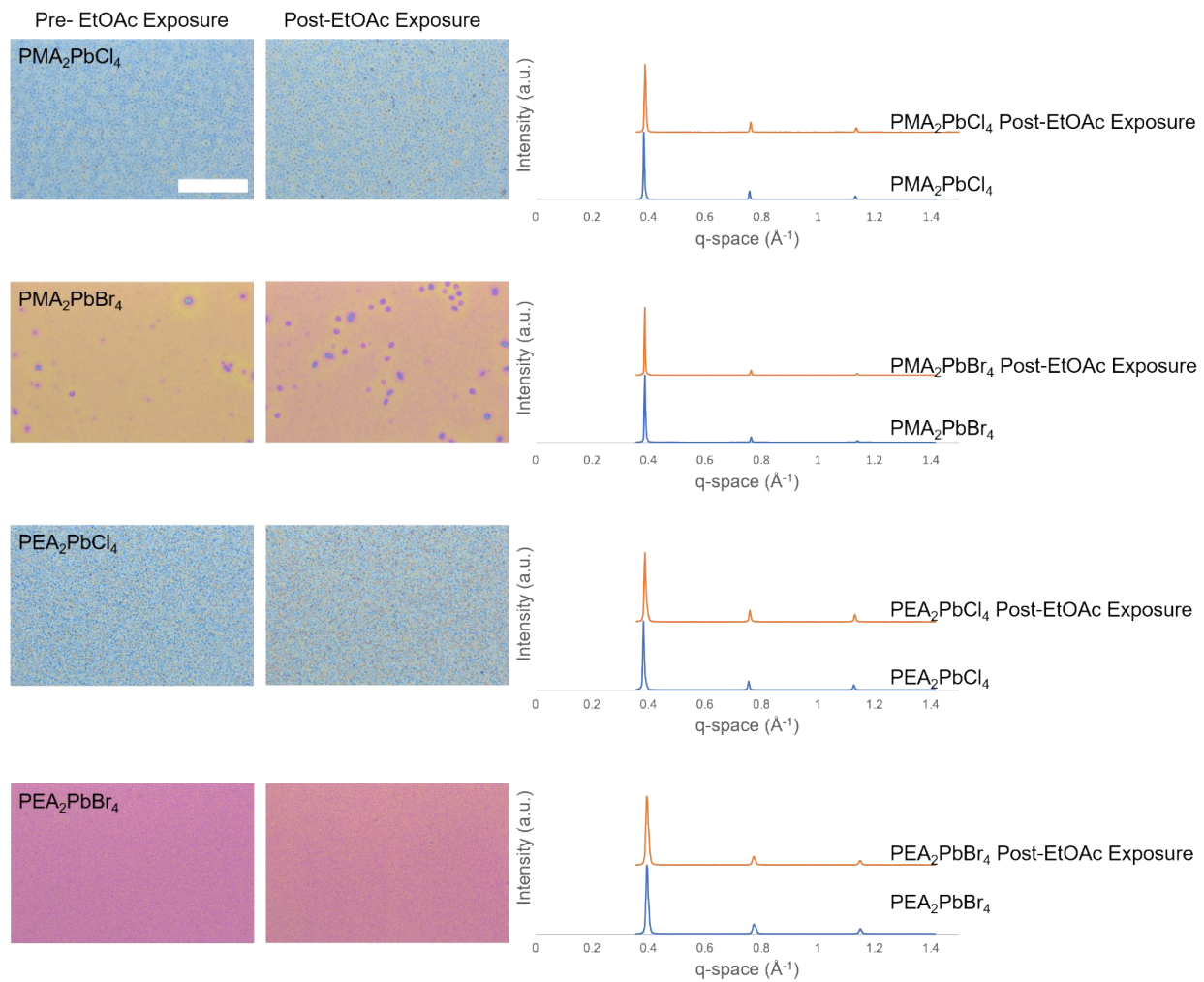
SI Figure 2: Unit cells of $\text{PMA}_2\text{PbCl}_4$, $\text{PMA}_2\text{PbBr}_4$, $\text{PEA}_2\text{PbCl}_4$, and $\text{PEA}_2\text{PbBr}_4$ and their respective diffraction patterns compared to simulated patterns [1], [2], [3], [4]



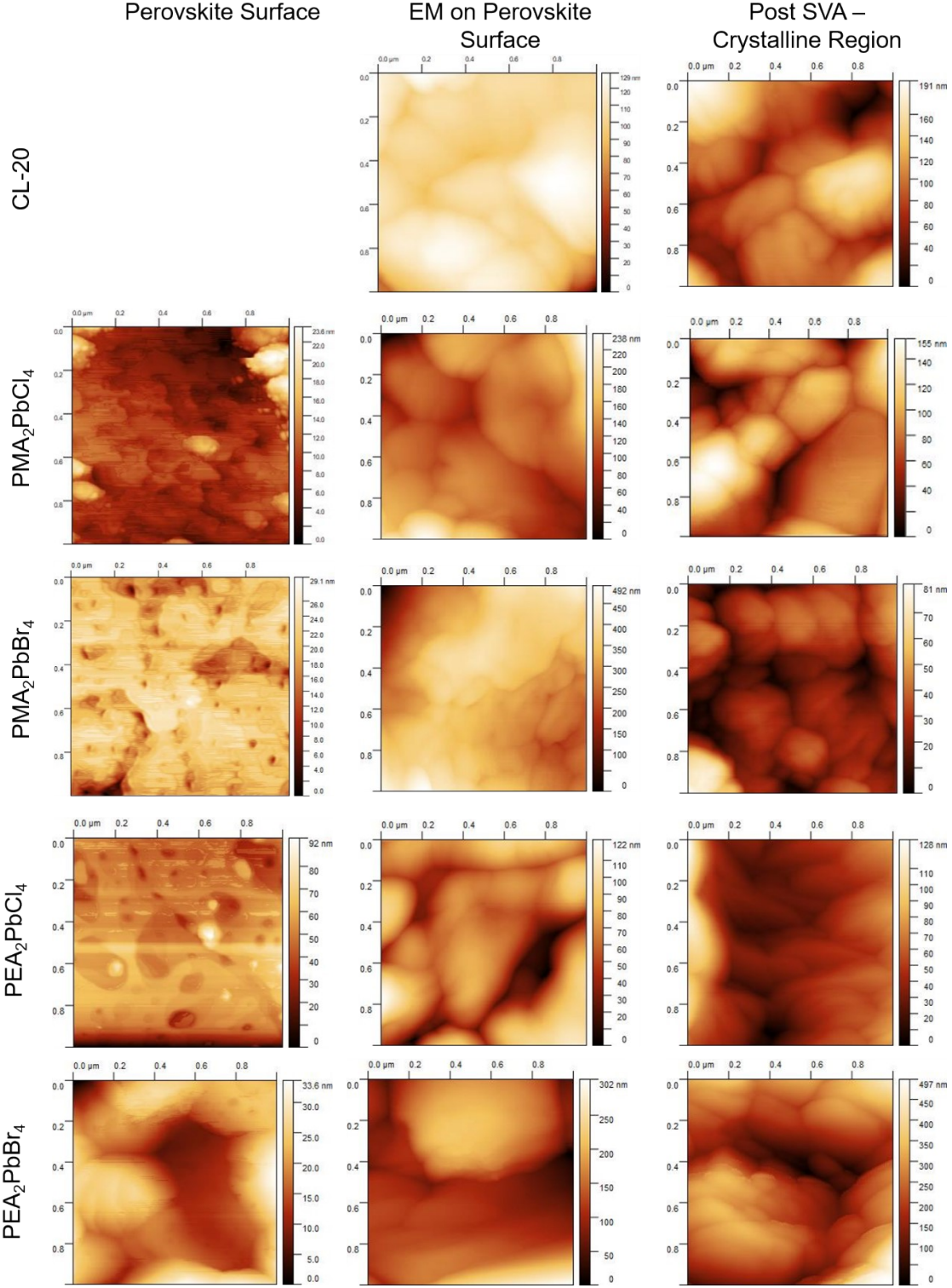
SI Figure 3: Relative orientation of benzene rings in PMA-based vs. PEA-based perovskite thin films.

SI Table 1: Calculations of ligand density for perovskite surfaces of interest. Bolded values indicate dimensions used to calculate periodic unit cell present at the interface of each perovskite.

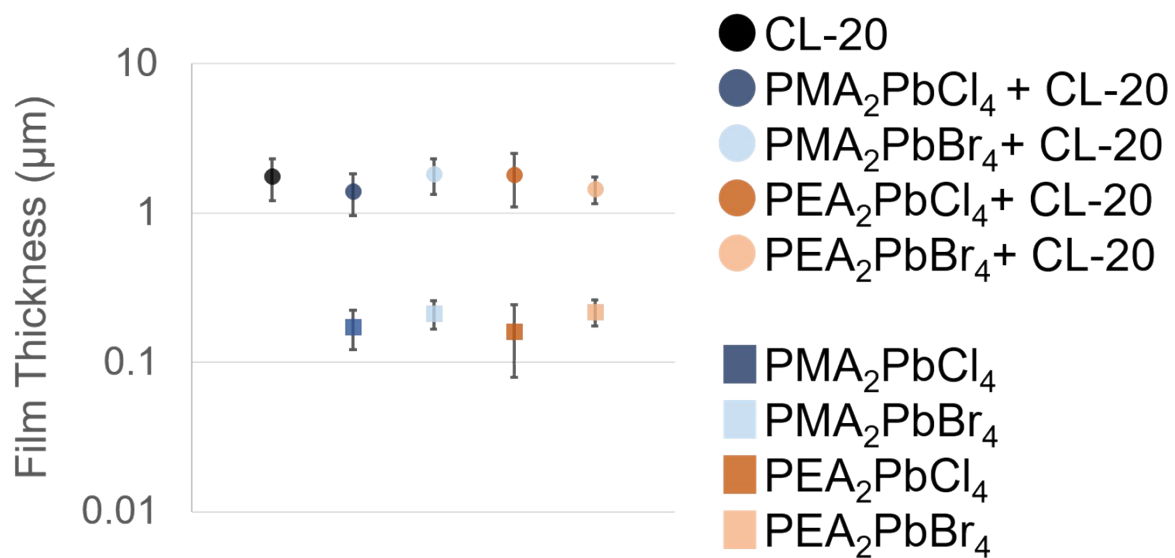
Perovskite	CCDC Deposition ID	a	b	c	Area (Å ²)	# of ligands	Ligand density (ligand/Å ²)
PMA ₂ PbCl ₄	1042742	33.63500	7.81700	7.73700	60.4801	2	0.03307
PMA ₂ PbBr ₄	1542460	33.35290	8.14660	8.12320	66.1765	2	0.03022
PEA ₂ PbCl ₄	1498513	11.11520	11.20480	17.59090	124.544	4	0.03212
PEA ₂ PbBr ₄	754084	11.61500	11.62750	17.57510	135.053	4	0.02962



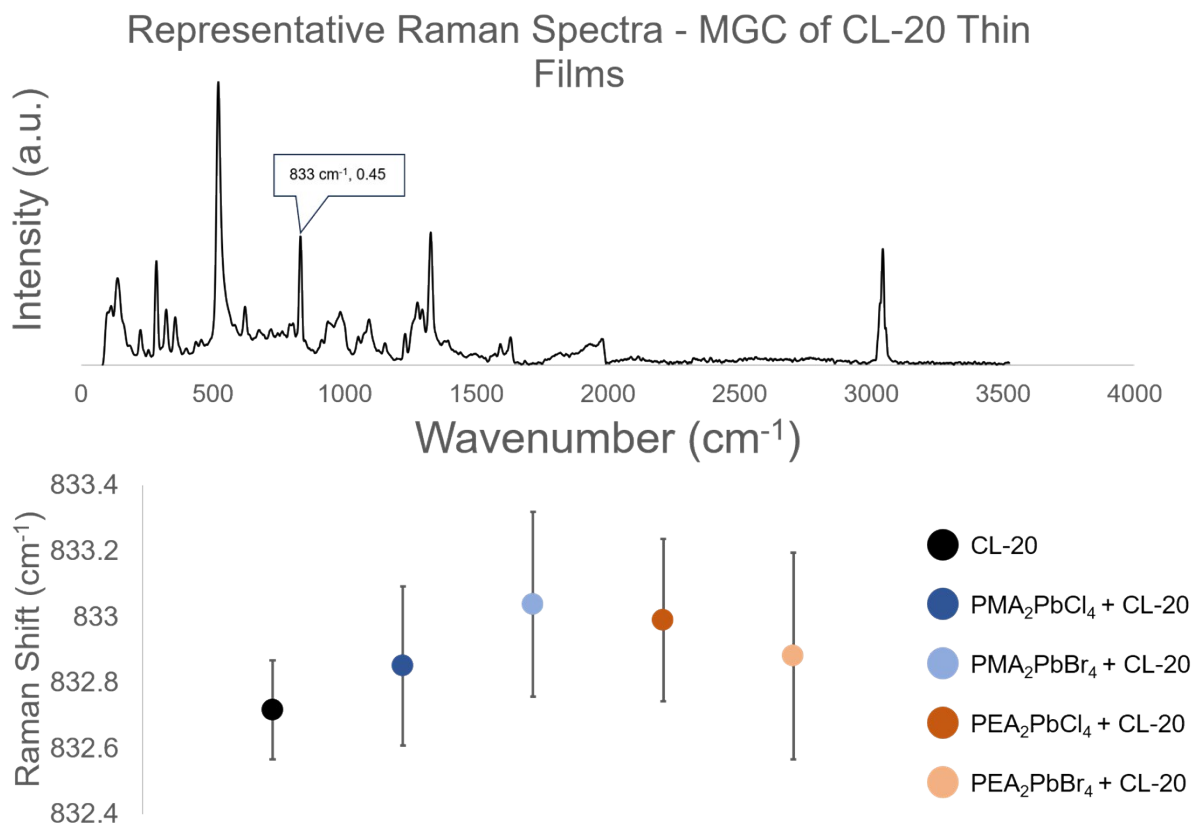
SI Figure 4: Optical images and x-ray diffraction patterns for perovskite films prior to and after exposure to ethyl acetate. Scale bar is the same for all images = 200 μm .



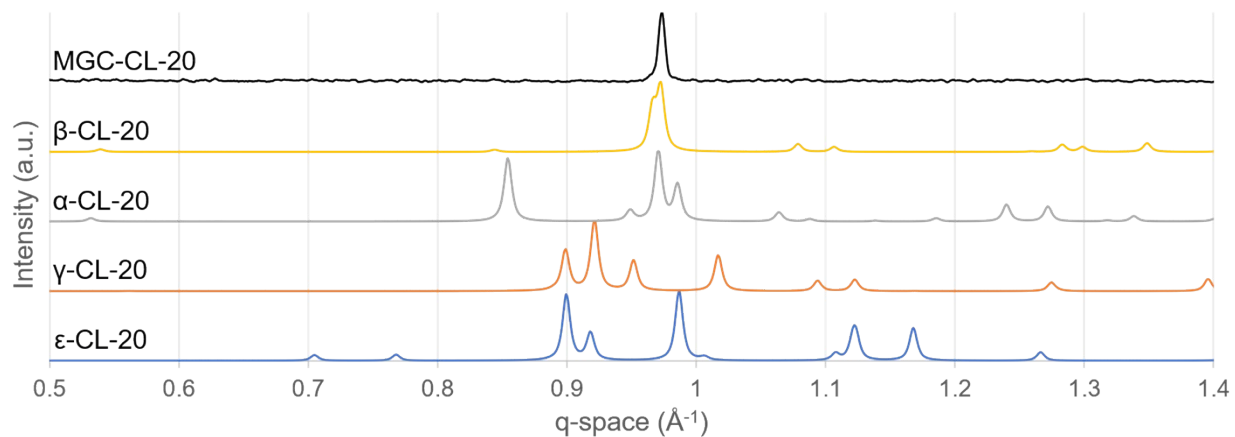
SI Figure 5: Atomic force microscopy of 2D MHP surfaces (left column), 2D MHP/CL-20 bilayer (middle column), and 2D MHP/CL-20 bilayer film after SVA (right column).



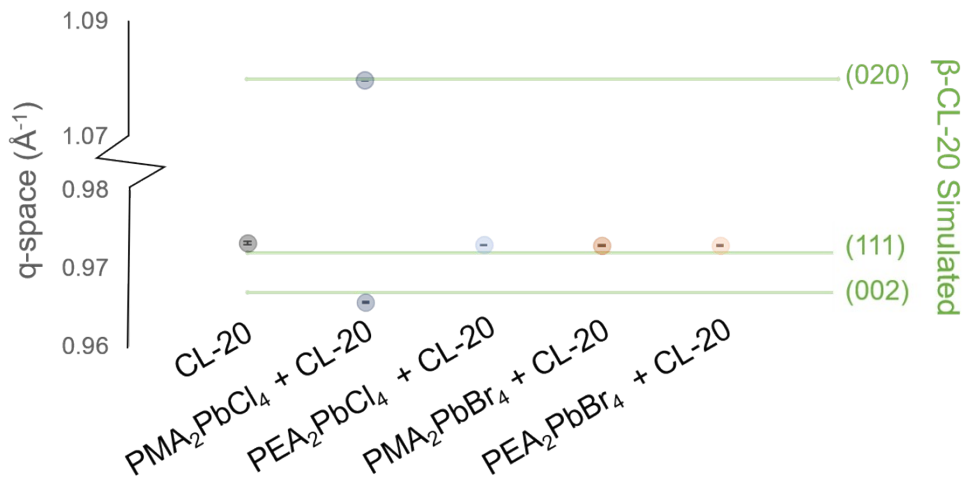
SI Figure 6: Film thickness measurements of 2D MHP (squares) and 2D MHP/CL-20 bilayer films (circles).



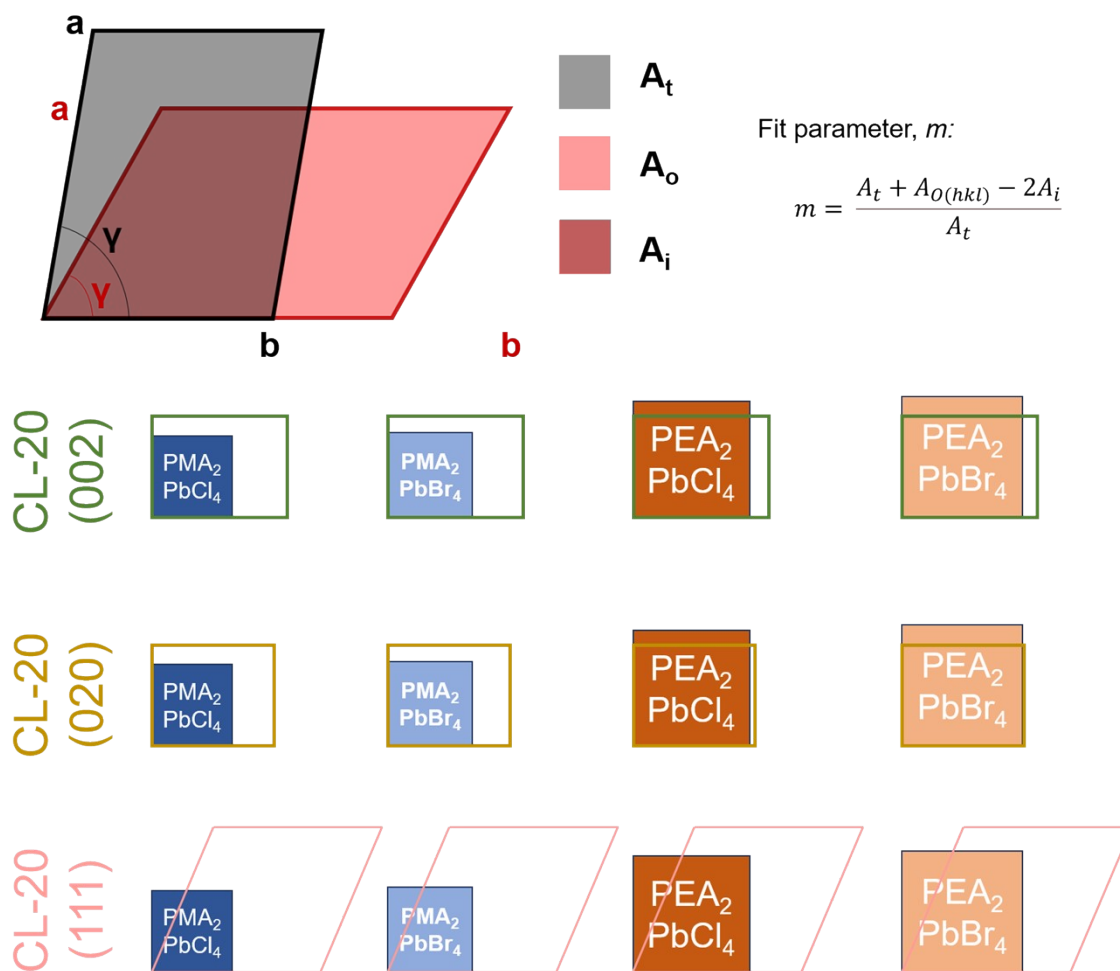
SI Figure 7: Representative Raman spectrum for CL-20 with peak at ~ 833 cm⁻¹ highlighted as this indicates crystallization of the β -CL-20 polymorph. Average peak location of perovskite/CL-20 bilayer films shows no significant peak shift due to interfacial interactions.



SI Figure 8: Representative XRD spectra of MGC-CL-20 relative to simulated patterns of three polymorphic (β , γ , ϵ) and one hydrate (α) structure of CL-20.[5], [6], [7] Confirmation of β -CL-20 crystallization with high degree of orientation in the MGC films.

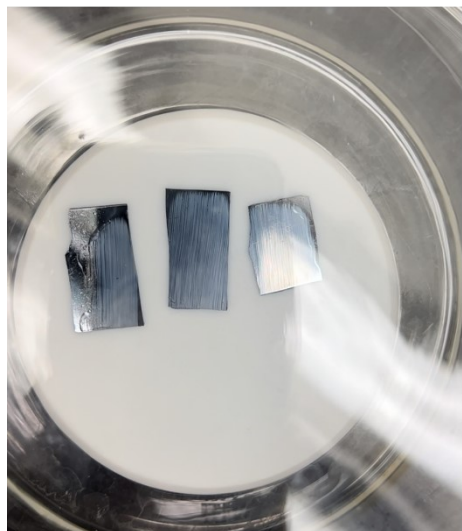


SI Figure 9: Average CL-20 peak location is tabulated for each bilayer pair relative to control MGC-CL-20 (black). Sample size = 3.

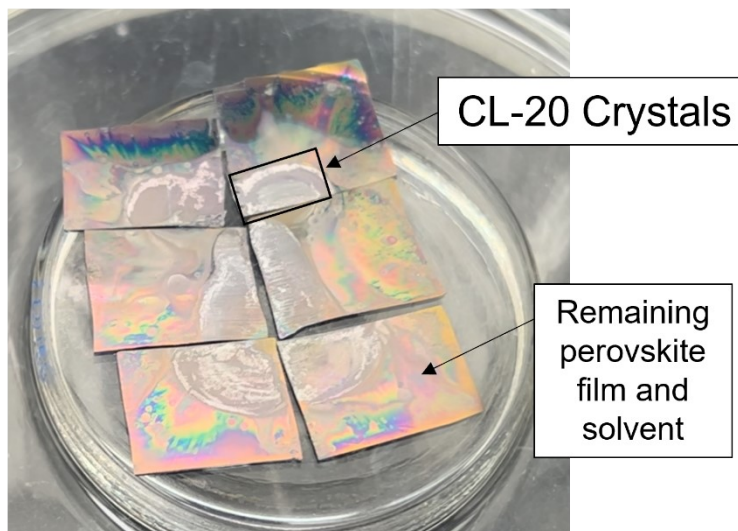


SI Figure 10: Fit parameter definition and calculation. Overlay of interfacial unit cells of (1x1) unit cell perovskite surfaces with crystallographic planes ((002), (020), and (111)) of β -CL-20. Adapted from [8].

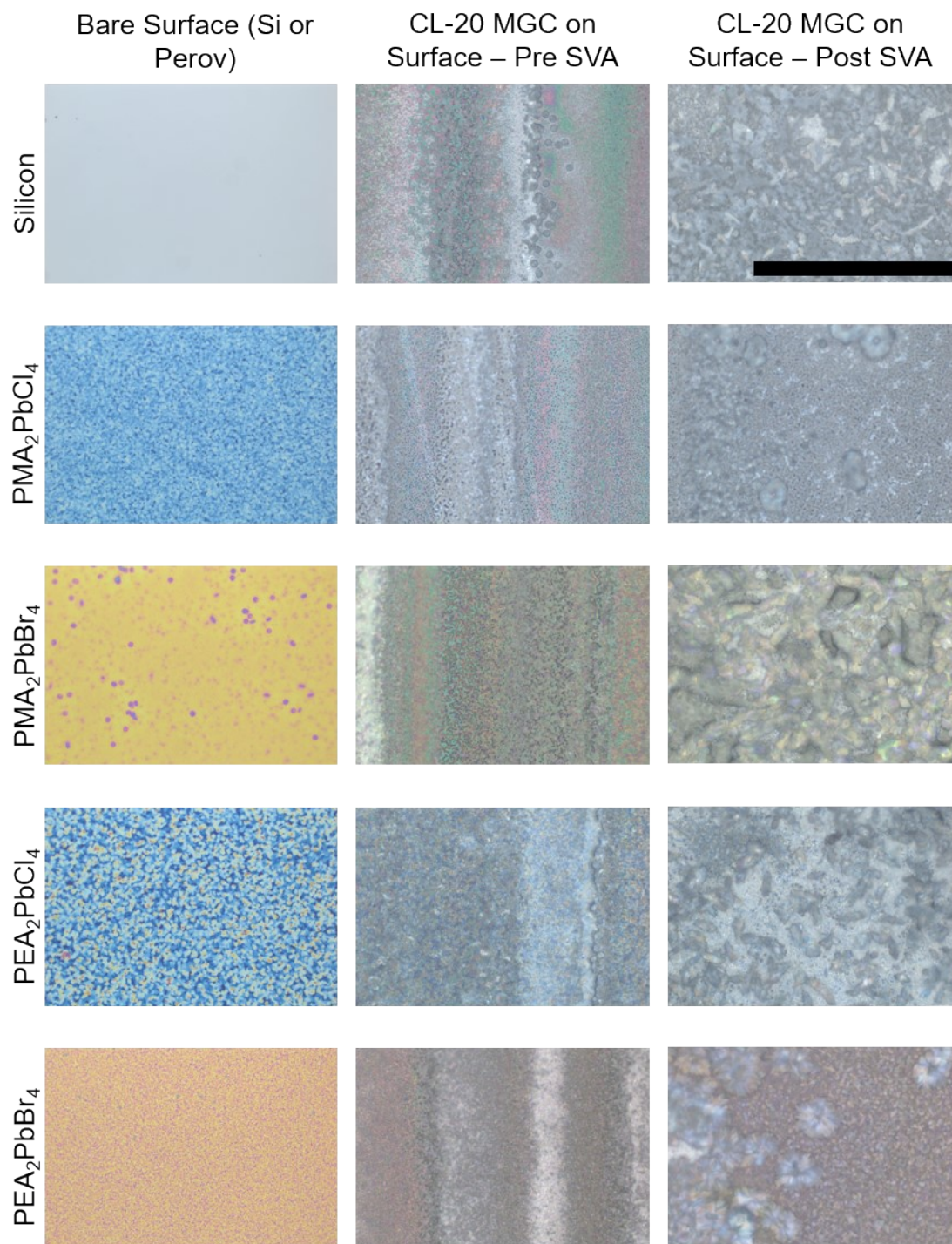
MGC Films in SVA chamber during onset of dissolution



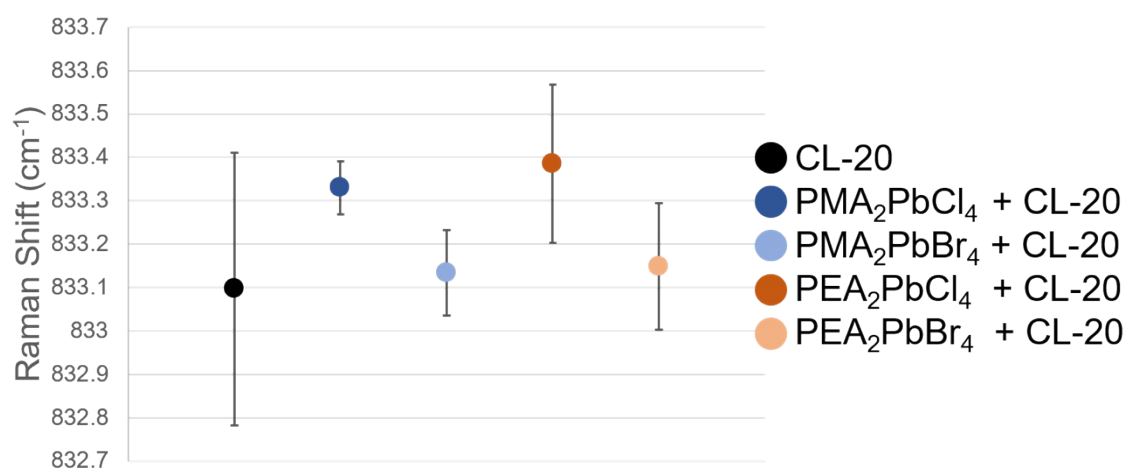
Films post SVA – accumulation of crystals in smaller area



SI Figure 11: Accumulation of CL-20 crystals during recrystallization after SVA. CL-20 crystals indicated in black box. Colorful area contains remaining perovskite film and residual solvent.



SI Figure 12: Optical images of perovskite surfaces (column 1), perovskite + CL-20 bilayer films after MGC (column 2), and perovskite + CL-20 bilayer films after MGC and SVA (column 3). Scale bar = 200 μm .



SI Figure 13: Average Raman shift of the 833 cm⁻¹ peak (associated with β -CL-20) after SVA in EtOAc. (n=3)

Appendix References:

- [1] W. Q. Liao *et al.*, "A lead-halide perovskite molecular ferroelectric semiconductor," *Nature Communications* 2015 6:1, vol. 6, no. 1, pp. 1–7, May 2015, doi: 10.1038/ncomms8338.
- [2] K. Du *et al.*, "Two-Dimensional Lead(II) Halide-Based Hybrid Perovskites Templated by Acene Alkylamines: Crystal Structures, Optical Properties, and Piezoelectricity," *Inorg Chem*, vol. 56, no. 15, pp. 9291–9302, Aug. 2017, doi: 10.1021/ACS.INORGCHEM.7B01094.
- [3] K. Thirumal *et al.*, "Morphology-Independent Stable White-Light Emission from Self-Assembled Two-Dimensional Perovskites Driven by Strong Exciton–Phonon Coupling to the Organic Framework," *Chemistry of Materials*, vol. 29, no. 9, pp. 3947–3953, May 2017, doi: 10.1021/ACS.CHEMMATER.7B00073.
- [4] K. Shibuya, M. Koshimizu, F. Nishikido, H. Saito, and S. Kishimoto, "Poly[bis(phenethylammonium) [di-bromido-plumbate(II)]-di- μ -bromido]," *Acta Crystallogr Sect E Struct Rep Online*, vol. 65, no. 11, pp. m1323–m1324, Oct. 2009, doi: 10.1107/S160053680903712X/ZQ2004ISUP2.HKL.
- [5] A. T. Nielsen *et al.*, "Synthesis of polyazapolycyclic caged polynitramines," *Tetrahedron*, vol. 54, no. 39, pp. 11793–11812, Sep. 1998, doi: 10.1016/S0040-4020(98)83040-8.
- [6] Y. Yu, S. Jin, J. Zhu, L. Li, S. Chen, and Q. Shu, "Crystal structure of 2,4,6,8,10,12-hexanitro-2,4,6,8,10,12-hexaazatetracyclo[5·5·0·05·9·03·11]dodecane 1/3 hydrate, C₆H₈N₁₂O₁₃," *Zeitschrift für Kristallographie - New Crystal Structures*, vol. 231, no. 2, pp. 491–492, Jun. 2016, doi: 10.1515/NCRS-2015-0156/DOWNLOADASSET/SUPPL/NCRS-2015-0156_SUPPL.CIF.
- [7] N. B. Bolotina, M. J. Hardie, R. L. Speer, and A. A. Pinkerton, "Energetic materials: Variable-temperature crystal structures of γ - and ϵ -HNIW polymorphs," *J Appl Crystallogr*, vol. 37, no. 5, pp. 808–814, Oct. 2004, doi: 10.1107/S0021889804017832.
- [8] J. T. Dull *et al.*, "Thin-Film Organic Heteroepitaxy," *Advanced Materials*, p. 2302871, 2023, doi: 10.1002/ADMA.202302871.